

# Deformed shell model results for two neutrino positron double beta decay of $^{84}\text{Sr}$

R. Sahu<sup>1</sup>, and V.K.B. Kota<sup>2,3</sup>

<sup>1</sup>*Physics Department, Berhampur University, Berhampur 760 007, Orissa, India*

<sup>2</sup>*Physical Research Laboratory, Ahmedabad 380 009, India*

<sup>3</sup>*Department of Physics, Laurentian University, Sudbury, ON P3E 2C6, Canada*

## Abstract

Half-lives  $T_{1/2}^{2\nu}$  for two neutrino positron double beta decay modes  $\beta^+\text{EC}/\text{ECEC}$  are calculated for  $^{84}\text{Sr}$ , a nucleus of current experimental interest, within the framework of the deformed shell model based on Hartree-Fock states employing a modified Kuo interaction in  $(^2p_{3/2}, ^1f_{5/2}, ^2p_{1/2}, ^1g_{9/2})$  space. For a reasonable description of the spectra of  $^{84}\text{Sr}$  and  $^{84}\text{Kr}$  and to generate allowed GT strengths, the single particle energies of the proton and neutron  $^1g_{9/2}$  orbitals, relative to the  $^2p_{3/2}$  orbital energy, are chosen to be (3.5 MeV, 1.5 MeV) for both  $^{84}\text{Sr}$  and  $^{84}\text{Rb}$  and (1.5 MeV, 1.5 MeV) for  $^{84}\text{Kr}$ . With this, the calculated half-lives for the  $\beta^+\text{EC}$  and  $\text{ECEC}$  modes are  $\sim 10^{26}\text{yr}$  and  $\sim 4 \times 10^{24}\text{yr}$  respectively.

PACS numbers: 23.40.Hc, 21.10.Tg, 21.60.Jz, 27.50.+e

## I. INTRODUCTION

Double beta decay (DBD) is a rare weak interaction process in which two identical nucleons inside the nucleus undergo decay either with the emission of two neutrinos or without any neutrinos. The two neutrino double beta decay ( $2\nu\beta^-\beta^-$ ) which was first predicted long back by Meyer [1] has been observed experimentally in more than 10 nuclei [2, 3]. In contrast, the positron decay modes, i.e.  $2\nu\beta^+\beta^+/\beta^+\text{EC}/\text{ECEC}$  decay modes (hereafter, all these three combined is called  $2\nu e^+\text{DBD}$ ) are not yet observed experimentally (exception being  $^{130}\text{Ba}$  decay derived from geochemical methods [4]). However, in the last few years there are serious attempts, using direct counting methods, to measure half-lives for  $2\nu e^+\text{DBD}$  modes in many nuclei ranging from  $^{64}\text{Zn}$  to  $^{132}\text{Ba}$  [5–9]. In the mass  $A=80$  region, the candidate nuclei for  $2\nu e^+\text{DBD}$  are  $^{78}\text{Kr}$ ,  $^{74}\text{Se}$  and  $^{84}\text{Sr}$ . For  $^{78}\text{Kr}$  and  $^{74}\text{Se}$  there are already some experimental efforts and following this, recently [10, 11] we have carried out calculations for these two nuclei using the so called deformed shell model (DSM). In addition we had previously attempted to study  $2\nu\beta^-\beta^-$  nuclear matrix elements for  $^{76}\text{Ge} \rightarrow ^{76}\text{Se}$  using DSM [12]. There was also an attempt for  $^{82}\text{Se} \rightarrow ^{82}\text{Kr}$  and it is seen that [13] DSM produces nuclear matrix elements within a factor of 2 the QRPA results given in [14].

Over the years, the DSM model based on Hartree-Fock states has been used to study with considerable success: (i) spectroscopic properties, such as band structures, shapes, nature of band crossings, electromagnetic transition probabilities and so on in  $A=64-80$  nuclei [15–20]; (ii)  $T = 1$  and  $T = 0$  bands in  $N=Z$  odd-odd nuclei and  $T = 1/2$  bands in odd- $A$  nuclei by including isospin projection [21–23]; (iii) transition matrix elements for  $\mu - e$  conversion in  $^{72}\text{Ge}$  [24] and in the analysis of data for inelastic scattering of electrons from  $fp$ -shell nuclei [25]; (iv)  $\beta$ -decay half lives, GT distributions and electron capture rates in  $N \sim Z$  nuclei in  $A=60-80$  region [10] and so on. It is seen that the predictions of DSM for  $2\nu e^+\text{DBD}$  half-lives for  $^{78}\text{Kr}$  are close to those of QRPA and PHFB models. For  $^{74}\text{Se}$  there are no other model predictions except those of DSM. See [10, 11] for details.

A group led by H.J. Kim at Korean KPNU facility has initiated DBD experiments for positron double beta decay (both  $2\nu$  and  $0\nu$ ) in  $^{84}\text{Sr}$  using  $\text{SrCl}_2$  crystals [26, 27]. Prompted by these efforts, we have carried out DSM calculations, extending the studies in [10, 11] further, for  $2\nu e^+\text{DBD}$  half-lives for  $^{84}\text{Sr}$  nucleus and the results are reported in this paper. It should be pointed out that there are no theoretical results available in literature for this

nucleus. Just as with  $^{78}\text{Kr}$  and  $^{74}\text{Se}$ , we have undertaken the  $2\nu e^+\text{DBD}$  study of  $^{84}\text{Sr}$  as it was already shown that DSM model describes very well [28] the low-lying bands in this nucleus. Also as we shall discuss ahead, the proton and neutron single particle energies (spe) of the  $1g_{9/2}$  orbital play an important role in describing the spectroscopic results of  $^{84}\text{Kr}$  and in determining the  $^{84}\text{Sr} \rightarrow ^{84}\text{Kr} 2\nu e^+\text{DBD}$  half lives. Now we will give a preview.

In Section II given is, for completeness, a brief discussion of DSM model and the formalism for calculating  $2\nu e^+\text{DBD}$  half-lives. Spectroscopic results for  $^{84}\text{Sr}$  and  $^{84}\text{Kr}$  are given in Section III. In Section IV, DSM results for  $2\nu e^+\text{DBD}$  half lives are discussed and also given here are some concluding remarks.

## II. $2\nu e^+\text{DBD}$ HALF-LIVES AND DEFORMED SHELL MODEL

Half-life for the  $2\nu e^+\text{DBD}$  decay modes for the  $0_I^+ \rightarrow 0_F^+$  transitions, is given by [29],

$$[T_{1/2}^{2\nu}(k)]^{-1} = G_{2\nu}(k) |M_{2\nu}|^2 \quad (1)$$

where  $k$  denotes the modes  $\beta^+\beta^+$ ,  $\beta^+\text{EC}$  and  $\text{ECEC}$ . The kinematical factors  $G_{2\nu}(k)$  are independent of nuclear structure and they can be calculated with good accuracy [29, 30]. On the other hand, the nuclear transition matrix elements (NTME)  $M_{2\nu}$  are nuclear model dependent and they are given by [29, 31],

$$M_{2\nu} = \sum_N \frac{\langle 0_F^+ || \sigma\tau^- || 1_N^+ \rangle \langle 1_N^+ || \sigma\tau^- || 0_I^+ \rangle}{[E_0 + E_N - E_I]} \quad (2)$$

where  $|0_I^+\rangle$ ,  $|0_F^+\rangle$  and  $|1_N^+\rangle$  are the initial, final and virtual intermediate states respectively and  $E_N(E_I)$  is the energy of the intermediate (initial) nucleus. Similarly,  $E_0 = \frac{1}{2}W_0$  where  $W_0$  is the total energy released for different  $2\nu e^+\text{DBD}$  modes. As given in [31–33],  $W_0(\beta^+\beta^+) = Q_{\beta^+\beta^+} + 2m_e$ ,  $W_0(\beta^+\text{EC}) = Q_{\beta^+\text{EC}} + e_b$  and  $W_0(\text{ECEC}) = Q_{\text{ECEC}} - 2m_e + e_{b1} + e_{b2}$ . The  $Q$ -values for different  $2\nu e^+\text{DBD}$  modes are [31]:  $Q_{\beta^+\beta^+} = M(A, Z) - M(A, Z - 2) - 4m_e$ ,  $Q_{\beta^+\text{EC}} = M(A, Z) - M(A, Z - 2) - 2m_e$  and  $Q_{\text{ECEC}} = M(A, Z) - M(A, Z - 2)$ . Here  $M$  denotes the neutral atomic mass (available for example from the tabulations in [34]) and  $e_b$  is the binding energy of the captured atomic electron. Energies in the denominator in Eq. (2) are taken in the units of electron mass. With the atomic mass difference being 1787 keV for  $^{84}\text{Sr}$  decay, it should be clear that the  $\beta^+\beta^+$  DBD mode is forbidden (as the  $Q$ -value will be negative) for  $^{84}\text{Sr}$ . For  $\beta^+\text{EC}$  and

ECEC modes, one and two K shell electron capture respectively are considered. The binding energy for the K shell electrons is taken from [35].

In DSM, for a given nucleus, starting with a model space consisting of a given set of single particle (sp) orbitals and effective two-body Hamiltonian, the lowest prolate and oblate intrinsic states are obtained by solving the Hartree-Fock (HF) single particle equation self-consistently. Excited intrinsic configurations are obtained by making particle-hole excitations over the lowest intrinsic state. These intrinsic states will not have good angular momentum and hence good angular momentum states are obtained by angular momentum projection from these intrinsic states. The normalized states of good angular momentum projected from the intrinsic state  $\chi_K(\eta)$  can be written in the form

$$\psi_{MK}^J(\eta) = \frac{2J+1}{8\pi^2\sqrt{N_{JK}}} \int d\Omega D_{MK}^{J*}(\Omega) R(\Omega) |\chi_K(\eta)\rangle \quad (3)$$

where  $N_{JK}$  is the normalization constant given by

$$N_{JK} = \frac{2J+1}{2} \int_0^\pi d\beta \sin \beta d_{KK}^J(\beta) \langle \chi_K(\eta) | e^{-i\beta J_y} | \chi_K(\eta) \rangle . \quad (4)$$

In Eq. (3)  $\Omega$  represents the Euler angles  $(\alpha, \beta, \gamma)$ ,  $R(\Omega)$  which is equal to  $\exp(-i\alpha J_z)\exp(-i\beta J_y)\exp(-i\gamma J_z)$  represents the general rotation operator. In general the projected states with same  $J$  but coming from different intrinsic states will not be orthogonal to each other. Hence they are orthonormalized and then band mixing calculations are performed. DSM is well established to be a successful model for transitional nuclei (with  $A=64-80$ ) when sufficiently large number of intrinsic states are included in the band mixing calculations. Performing DSM calculations for the parent, daughter and the intermediate odd-odd nucleus (here we need only the  $1^+$  states) and then using the DSM wavefunctions, the  $\sigma\tau^-$  matrix elements in Eq. (2) are calculated. For further details of DSM see [10].

Let us add that the recently introduced projected configuration interaction (PCI) model of Horoi et al [36, 37] and the projected shell model (PSM) of Sun et al [38–40] are quite similar to DSM (PCI may be better for quasi-spherical nuclei and PSM includes BCS correlations from the beginning).

### III. SPECTROSCOPIC RESULTS FOR $^{84}\text{Sr}$ AND $^{84}\text{Kr}$

#### A. $^{84}\text{Sr}$

In the DSM calculations for the structure of the nuclei  $^{84}\text{Sr}$ ,  $^{84}\text{Rb}$  and  $^{84}\text{Kr}$  and for  $^{84}\text{Sr}$   $2\nu$   $e^+\text{DBD}$  half-lives presented in section IV, we have used a modified Kuo effective interaction [41] in the  $(^2p_{3/2}, ^1f_{5/2}, ^2p_{1/2}, ^1g_{9/2})$  space with  $^{56}\text{Ni}$  as the inert core. The spe of these orbitals are taken as 0.0, 0.78, 1.08 and 3.5 MeV respectively in a first set of calculations and in the next set of calculations, the  $^1g_{9/2}$  energy for the protons and/or neutrons is changed to 1.5 MeV for reasons discussed in detail ahead. DSM with modified Kuo effective interaction has been quite successfully used by us in describing many important features of nuclei in  $A \sim 60\text{-}80$  region. In particular, shape coexistence in spectra, observed  $B(E2)$  values, identical bands, band crossings, and deformations in  $^{76,78,80,82,84}\text{Sr}$  isotopes are well described by DSM [17, 28]. First we will describe briefly the earlier spectroscopic results for  $^{84}\text{Sr}$ .

Starting with the modified Kuo interaction and  $^2p_{3/2}$ ,  $^1f_{5/2}$ ,  $^2p_{1/2}$ ,  $^1g_{9/2}$  spe (both for protons and neutrons) to be 0.0, 0.78, 1.08 and 3.5 MeV respectively, DSM calculations have been carried out for  $^{84}\text{Sr}$  in [28]. Here, first axially symmetric HF calculations are performed and the lowest prolate HF intrinsic state is obtained. The reason for neglecting the oblate states has been discussed in detail in [19]. The lowest HF sp spectrum for  $^{84}\text{Sr}$  is shown in Fig. 1a; note that the HF sp states with a given  $k$  values will be doubly degenerate. By particle-hole excitations from the lowest intrinsic state shown in Fig. 1a, excited intrinsic states are generated. In the band mixing calculations a limited number of five configurations are taken and they are: (i) ground  $K^\pi = 0^+$  intrinsic state; (ii) two excited  $K^\pi = 0^+$  intrinsic states obtained by exciting two or four protons into the  $k$  states arising out of the  $^1g_{9/2}$  orbit; (iii) a  $K^\pi = 8^+$  intrinsic state obtained by exciting two valence neutrons into  $k = 7/2^+$  and  $9/2^+$  states; (iv) a  $K^\pi = 2^+$  intrinsic state obtained by exciting a valence proton from  $k = 5/2^-$  into  $1/2^-$  state. As discussed in detail in [28], the band mixing calculations reproduce the observed data quite well. Figure 2 shows the calculated and experimental spectra. The DSM results in Fig. 2 are slightly different from those in Fig. 2a of [28] where the so called tagged HF calculation is done (in the present calculations, just as in [10, 11], no tagging has been done). The results for  $10^+$  and  $12^+$  levels are in better

agreement with data compared to the earlier results in [28]. The two lowest excited  $8^+$  bands in Fig. 2 are established by experiments [42, 43] to be two neutron and two proton aligned bands respectively and DSM reproduces this structure. Similarly, the observed  $B(E2)$  values and also the excited  $2^+$  band are well described. All these confirm that DSM gives good spectroscopic results for  $^{84}\text{Sr}$ .

In the  $2\nu e^+\text{DBD}$  decay, the intermediate nucleus is  $^{84}\text{Rb}$ . Fig. 1b gives the HF spectrum for  $^{84}\text{Rb}$  (for completeness we also show the HF spectrum for  $^{84}\text{Kr}$  in Fig. 1c). As we can see from Fig. 1, in the DBD process, in the lowest order, the valence proton from the  $5/2^-$  orbit in  $^{84}\text{Sr}$  will go to the unoccupied neutron  $7/2^+$  orbit in  $^{84}\text{Rb}$ . This gives a negative parity state for  $^{84}\text{Rb}$  and this is not allowed by GT. Hence an intrinsic state with a proton in  $5/2^+$  in  $^{84}\text{Sr}$  is needed to generate allowed GT matrix elements. However the intensity of this configuration will be small in the  $^{84}\text{Sr}$  ground state. Thus the GT matrix elements will be small for  $^{84}\text{Sr}$  to  $^{84}\text{Rb}$ . Therefore we need to reduce the neutron  $^1g_{9/2}$  spe for these two nuclei so that the negative parity neutron sp states will be near the Fermi surface. As a result we will be generating many low-lying  $K^\pi = 1^+$  levels in  $^{84}\text{Rb}$  and there will be large GT matrix elements for  $^{84}\text{Sr}$  to  $^{84}\text{Rb}$  (similarly also for  $^{84}\text{Rb}$  to  $^{84}\text{Kr}$ ). Following this, we have considered proton  $^1g_{9/2}$  spe  $\epsilon^{(p)}(^1g_{9/2}) = 3.5$  MeV and neutron  $^1g_{9/2}$  spe  $\epsilon^{(n)}(^1g_{9/2}) = 1.5$  MeV. The HF sp spectrum for this choice is shown in Fig. 3a. Starting with the lowest configuration shown in Fig. 3a, five more excited configurations are considered in the band mixing calculations as before for  $^{84}\text{Sr}$ . Fig. 2 shows that practically there is no effect of the change in  $\epsilon^{(n)}(^1g_{9/2})$  on the spectrum (also wavefunctions and hence the results in [28] are well preserved). The reason being that there is essentially no change in the proton and neutron occupancies. In Fig. 2, deviations of the results of the earlier calculation from the present calculation are shown in the parentheses with an asterisk. Deviations below 50 keV are not shown.

In conclusion, for  $^{84}\text{Sr}$  and  $^{84}\text{Rb}$  nuclei, for DSM calculations we employ the spe for  $^2p_{3/2}$ ,  $^1f_{5/2}$  and  $^2p_{1/2}$  orbitals (same spe for both protons and neutrons) to be 0.0, 0.78, 1.08 MeV respectively while  $[\epsilon^{(p)}(^1g_{9/2}), \epsilon^{(n)}(^1g_{9/2})] = [3.5, 1.5]$  MeV. Now we will consider  $^{84}\text{Kr}$  where there were no earlier DSM results.

## B. $^{84}\text{Kr}$

Employing the same set of spe as chosen for  $^{84}\text{Sr}$  and  $^{84}\text{Rb}$ , the lowest prolate HF intrinsic state is obtained for  $^{84}\text{Kr}$ ; note that as above  $\epsilon^{(p)}(^1g_{9/2}) = 3.5$  MeV and  $\epsilon^{(n)}(^1g_{9/2}) = 1.5$  MeV. Then the HF sp spectrum in Fig. 1c remains unchanged except that the HF neutron  $1g_{9/2}$   $k$ -states move down in energy by 2 MeV. By particle-hole excitations from the lowest intrinsic state, excited intrinsic states are generated for  $^{84}\text{Kr}$  and band mixing calculations are carried out using lowest 15 configurations. The observed lowest  $6^+$ ,  $8^+$  and  $10^+$  states are two-proton aligned states and similarly the  $8_2^+$  and  $10_2^+$  are two-neutron aligned bands. It is seen that the calculated two-proton aligned band is high (by more than 1 MeV) compared to experiment. Also the  $6^+$  level produces weak  $B(E2)$  for  $6_1^+ \rightarrow 4_1^+$ ; the calculated value is 0.2 W.u. while 6.9 W.u. is the data value (see Table 1). In order to bring the two-proton aligned band head to be close to data, it is necessary to lower the  $\epsilon^{(p)}(^1g_{9/2})$  energy to 1.5 MeV in addition to using  $\epsilon^{(n)}(^1g_{9/2}) = 1.5$  MeV. The HF sp spectrum with  $[\epsilon^{(p)}(^1g_{9/2}), \epsilon^{(n)}(^1g_{9/2})] = [1.5, 1.5]$  MeV is shown in Fig. 3c and the energy spectrum is shown in Fig. 4. In the DSM calculations, starting with the lowest configuration shown in Fig. 3c, 15 excited configurations are considered for band mixing. It is seen from Fig. 4 that the two-proton aligned band is in reasonable agreement with experiment. From Fig. 4 and also the  $B(E2)$  results in Table 1, we conclude that DSM gives a reasonably good description of the spectroscopy of  $^{84}\text{Kr}$  with the choice  $[\epsilon^{(p)}(^1g_{9/2}), \epsilon^{(n)}(^1g_{9/2})] = [1.5, 1.5]$  MeV. Let us add that the recent data on occupancies in  $^{76}\text{Ge}$  and  $^{76}\text{Se}$  do point out that  $[44, 45]$   $1g_{9/2}$  is probably much closer to the  $fp$  shell than anticipated in the past, thus justifying the lowering of the energies of proton and neutron  $1g_{9/2}$  orbitals. It is also plausible that part of the reason for these lower energies may be due to the neglect of excitations into  $1g_{7/2}$  and  $2d_{5/2}$  orbitals.

In conclusion, for  $^{84}\text{Kr}$  for DSM calculations we employ the spe for  $^2p_{3/2}$ ,  $^1f_{5/2}$  and  $^2p_{1/2}$  orbitals (same spe for both protons and neutrons) to be 0.0, 0.78, 1.08 MeV respectively while  $[\epsilon^{(p)}(^1g_{9/2}), \epsilon^{(n)}(^1g_{9/2})] = [1.5, 1.5]$  MeV.

#### IV. RESULTS FOR $2\nu$ $e^+$ DBD HALF LIVES AND CONCLUSIONS

Using the DSM wavefunctions,  $2\nu$   $\beta^+$ EC and ECEC half-lives for  $^{84}\text{Se} \rightarrow ^{84}\text{Kr}$  transitions are calculated and the results are shown in Table 2. In the DSM calculations for the intermediate nucleus  $^{84}\text{Rb}$ , 24  $K^\pi = 1^+$  bands are mixed and they span 3 MeV from the lowest  $K^\pi = 1^+$  band. The resulting 24  $1^+$  states are employed in Eq. (2) to calculate the GT matrix elements. We have verified that the inclusion of additional  $1^+$  states do not change significantly the half-life results. Further, the  $0^+$  ground state of  $^{84}\text{Sr}$  is generated by mixing 30 intrinsic states. Similarly for generating the  $0^+$  ground state of  $^{84}\text{Kr}$  11 intrinsic states are used in the DSM calculations. The Kinematical factors  $G_{2\nu}$  are taken from [30]. It is seen from Table 2 that the predicted half-lives are  $\sim 10^{25}\text{yr}$  and this should be of interest for future experiments. Instead of the choice  $[\epsilon^{(p)}(^1g_{9/2}), \epsilon^{(n)}(^1g_{9/2})] = [1.5, 1.5]$  MeV, if we use (3.5, 1.5) MeV for generating the ground state  $0^+$  of  $^{84}\text{Kr}$  just as the spe used for ( $^{84}\text{Sr}$ ,  $^{84}\text{Rb}$ ), the half-lives reduce by a factor  $\sim 2$  as shown in the brackets in Table 2. Let us add that the results in Table 2 are the first nuclear structure results for  $2\nu$   $\beta^+$ EC and ECEC half-lives for  $^{84}\text{Se} \rightarrow ^{84}\text{Kr}$ .

In conclusion, prompted by recent experimental interest in  $^{84}\text{Sr}$   $2\nu$   $e^+$ DBD and the results reported in [10, 11] for  $^{78}\text{Kr}$  and  $^{74}\text{Se}$  using the DSM model, we have carried out spectroscopic calculations and then the DBD half-lives calculations for  $^{84}\text{Sr} \rightarrow ^{84}\text{Kr}$ . We have shown that the DSM model gives reasonably good spectroscopy for both  $^{84}\text{Sr}$  and  $^{84}\text{Kr}$  by adjusting the spe of proton and neutron  $1g_{9/2}$  orbitals. Proceeding further we have presented the DSM results for half-lives for  $\beta^+$ EC and ECEC modes. These results should be a good guide for the experiments initiated by Kim et al [26, 27] at KPNU, Korea. Finally, formulation within DSM, for calculating  $0\nu$ DBD and  $0\nu$   $e^+$ DBD half lives is being developed and the results for  $^{84}\text{Sr}$   $0\nu$   $e^+$ DBD half lives will be reported in future.

#### Acknowledgments

Thanks are due to H.J. Kim for his interest in the results in the paper and for correspondence. Thanks are also due to P.C. Srivastava for help in preparing the figures. RS is



thankful to DST (India) for financial support.

---

- [1] M. Meyer, Phys. Rev. **48**, 512 (1935).
- [2] S.R. Elliott and P. Vogel, Annu. Rev. Nucl. Part. Sci. **52**, 115 (2002).
- [3] V.I. Tretyak and Y.G. Zdesenko, Atomic Data and Nuclear Data Tables **80**, 83 (2002).
- [4] A.P. Meshik, C.M. Hohenberg, O.V. Pravdivtseva, and Ya.S. Kapusta, Phys. Rev. C **64**, 035205 (2001).
- [5] P. Belli et al., Physics Letter **B658**, 193 (2008); preprint ROM2F/2007/13.
- [6] A.S. Barabash, Ph. Hubert, A. Nachab, and V. Umatov, Nucl. Phys. **A785**, 371 (2007).
- [7] Ju. M. Gavriljuk et al, Phys. At. Nucl. **69**, 2124 (2006); C. Sáenz et al, Phys. Rev. C **50**, 1170 (1994).
- [8] P. Belli et al., Astropart. Phys. **10**, 115 (1999).
- [9] R. Cerulli et al., Nucl. Instrum. Meth. Phys. Res. **A525**, 535 (2004).
- [10] S. Mishra, A. Shukla, R. Sahu, and V.K.B. Kota, Phys. Rev. C **78**, 024307 (2008).
- [11] A. Shukla, R. Sahu and V.K.B. Kota, Phys. Rev. C **80**, 057305 (2009).
- [12] R. Sahu, F. Šimkovic, and A. Faessler, J. Phys. G **25**, 1159 (1999).
- [13] R. Sahu, unpublished.
- [14] A. Bobyk et al., Nucl. Phys. **A669**, 221 (2000).
- [15] R. Sahu and S.P. Pandya, J. Phys. G **14**, L165 (1988).
- [16] R. Sahu and S.P. Pandya, Nucl. Phys. **A548**, 64 (1992).
- [17] K.C. Tripathy and R. Sahu, J. Phys. G **20**, 911 (1994).
- [18] R. Sahu and S.P. Pandya, Nucl. Phys. **A571**, 253 (1994).
- [19] K. C. Tripathy and R. Sahu, Nucl. Phys. **A597**, 177 (1996).
- [20] K.C. Tripathy and R. Sahu, Int. J. Mod. Phys. E **11**, 531 (2002).
- [21] R. Sahu and V.K.B. Kota, Phys. Rev. C **66**, 024301 (2002).
- [22] R. Sahu and V.K.B. Kota, C **67**, 054323 (2003).
- [23] S. Mishra, R. Sahu, and V.K.B. Kota, Prog. Theo. Phys. **118**, 59 (2007).
- [24] T.S. Kosmas, A. Faessler, and R. Sahu, Phys. Rev. C **68**, 054315 (2003).
- [25] R. Sahu, K.H. Bhatt, and D.P. Ahalpara, J. Phys. G **16**, 733 (1990).
- [26] [http://www.apctp.org/topical/2009/npap2009/Presentations/APCTP\\_NPAP2009\\_192\\_](http://www.apctp.org/topical/2009/npap2009/Presentations/APCTP_NPAP2009_192_)

- [27] H.J. Kim, private communication.
- [28] R. Sahu, Nucl. Phys. **A501**, 311 (1989).
- [29] M. Doi and T. Kotani, Prog. Theo. Phys. **87**, 1207 (1992).
- [30] F. Boehm and P. Vogel, *Physics of Massive Neutrinos* (Cambridge University Press, Cambridge, 1992).
- [31] M. Hirsch, K. Muto, T. Oda, H.V. Klapdor-Kleingrothaus, Z. Phys. **A347**, 151 (1994).
- [32] A. Shukla, P.K. Raina, R. Chandra, P.K. Rath, and J.G. Hirsch, Eur. Phys. J. **A23**, 235 (2005).
- [33] A. Shukla, P.K. Raina, and P.K. Rath, J. Phys. G: Nucl. Part. Phys. **34**, 549 (2007).
- [34] G. Audi, A. H. Wapstra, and C. Thibault, Nucl. Phys **A729**, 337 (2003).
- [35] <http://www.webelements.com/webelements/elements/text/periodic-table/bind.html>
- [36] Z. Gao and M. Horoi, Phys. Rev. C **79**, 014311 (2009).
- [37] Z. Gao, M. Horoi, and Y.S. Chen, Phys. Rev. C **80**, 034325 (2009).
- [38] K. Hara and Y. Sun, Int. J. Mod. Phys. E **4**, 637 (1995).
- [39] J.A. Sheikh and K. Hara, Phys. Rev. Lett. **82**, 3968 (1999).
- [40] Z.C. Gao, Y.S. Chen, and Y. Sun, Phys. Lett. **B634**, 195 (2006).
- [41] D.P. Ahalpara, K.H. Bhatt, and R. Sahu, J. Phys. G **11**, 735 (1985).
- [42] A. Dewald et al., Phys. Rev. C **25**, 226 (1982).
- [43] <http://www.nndc.bnl.gov/chart>
- [44] J.P. Schiffer et al., Phys. Rev. Lett. **100**, 112501 (2008).
- [45] B.P. Kay et al., Phys. Rev. C **79**, 021301(R) (2009).
- [46] J. K. Boheke et al., J. Phys. Chem. Ref. Data **34**, 57 (2005).

TABLE I:  $B(E2)$  values for  $^{84}\text{Kr}$  in Weisskopf units (W.u.). DSM results are compared with experimental results (called EXPT in the table) from [43]. The effective charges employed are  $e_p = 1.6e$  and  $e_n = 1.0e$  just as in the previous paper on  $^{84}\text{Sr}$  [28].

Transition	DSM	EXPT
$2_1^+ \rightarrow 0_1^+$	18.4	12
$4_1^+ \rightarrow 2_1^+$	28.9	15
$6_1^+ \rightarrow 4_1^+$	18.8	6.9
$2_1^+ \rightarrow 2_2^+$	3.2	13.3
$4_1^+ \rightarrow 2_2^+$	4	1.6
$2_3^+ \rightarrow 0_1^+$	1.6	3

TABLE II: Deformed Shell Model results for half-lives  $T_{1/2}^{2\nu}$  and the corresponding phase space factors  $G_{2\nu}$  for possible decay modes for  $^{84}\text{Sr} \rightarrow ^{84}\text{Kr}$ . Note that the natural abundance of  $^{84}\text{Sr}$  is 0.56% [46]. The  $G_{2\nu}$  and half-lives are calculated using  $g_A/g_V = 1$ . For half-lives given in the brackets see text.

Mode	$G_{2\nu}$ (in $\text{yr}^{-1}$ )	$T_{1/2}^{2\nu}$ (in yr) from DSM
$\beta^+\text{EC}$	$1.504 \times 10^{-24}$	$1.2 \times 10^{26}$ ( $5.41 \times 10^{25}$ )
ECEC	$4.367 \times 10^{-23}$	$4.16 \times 10^{24}$ ( $1.87 \times 10^{24}$ )

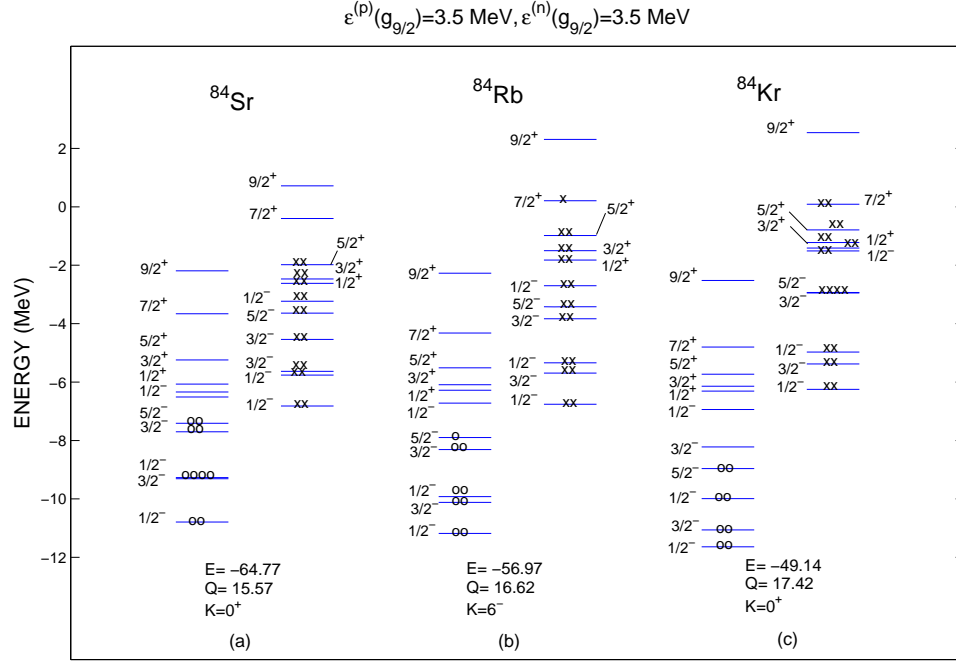


FIG. 1: HF single particle spectra for  $^{84}\text{Sr}$ ,  $^{84}\text{Rb}$  and  $^{84}\text{Kr}$  for  $\epsilon^{(p)}(^1g_{9/2}) = \epsilon^{(n)}(^1g_{9/2}) = 3.5 \text{ MeV}$ . In the figures circles represent protons and crosses represent neutrons. The Hartree-Fock energy ( $E$ ) in MeV, mass quadrupole moment ( $Q$ ) in units of the square of the oscillator length parameter and the total  $K$  quantum number of the lowest intrinsic states are given in the figure.

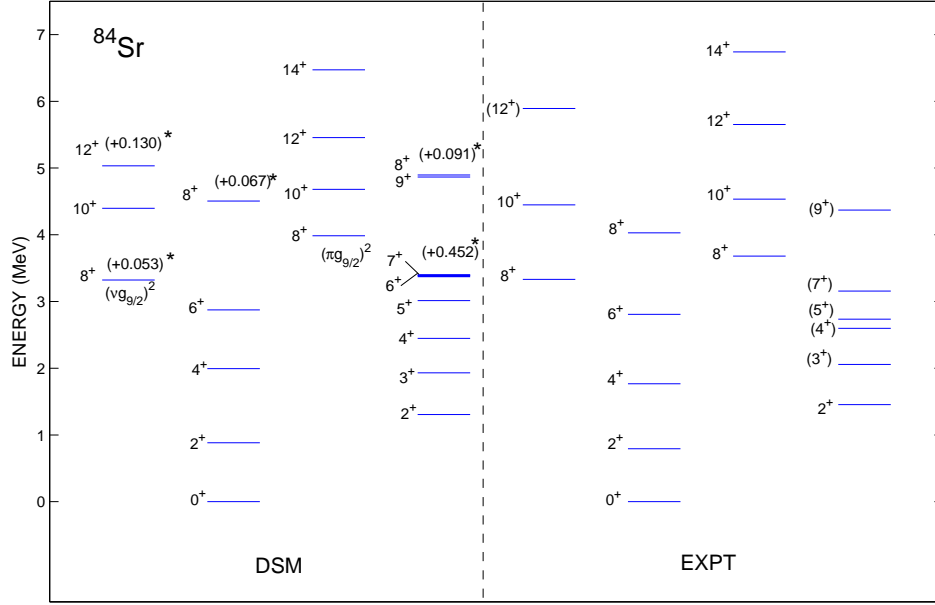


FIG. 2: (a) Calculated and (b) experimental spectra for  $^{84}\text{Sr}$ . Experimental data are from [42, 43]. Note that the DSM spectrum is obtained using  $[\epsilon^{(p)}(^1g_{9/2}), \epsilon^{(n)}(^1g_{9/2})] = [3.5, 1.5]\text{MeV}$ . The numbers in the brackets (over a few levels) indicate the difference between the calculated energies and those obtained with the choice  $[\epsilon^{(p)}(^1g_{9/2}), \epsilon^{(n)}(^1g_{9/2})] = [3.5, 3.5]\text{MeV}$ . See text for details.

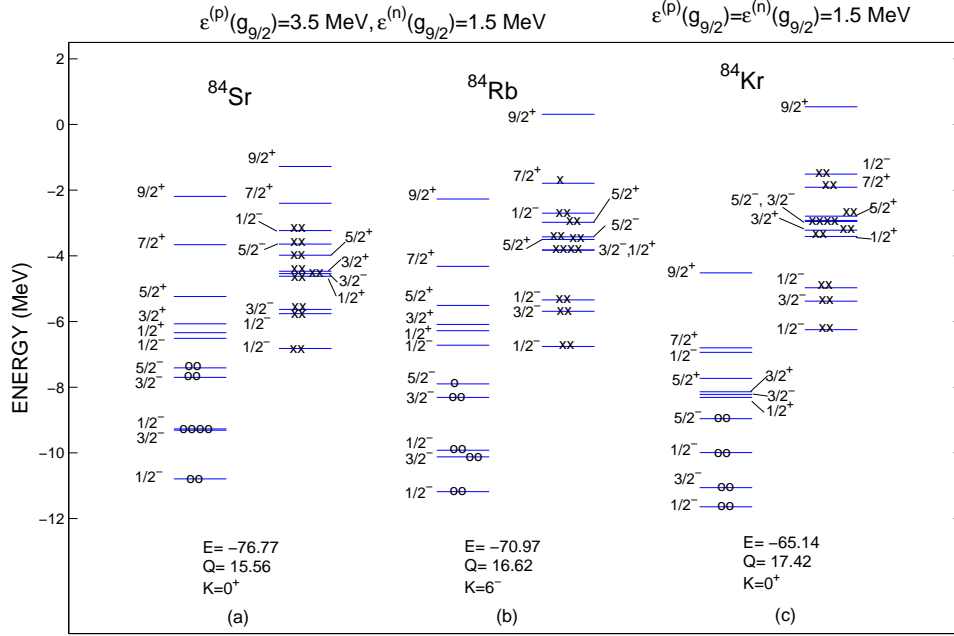


FIG. 3: HF single particle spectra for  $^{84}\text{Sr}$ ,  $^{84}\text{Rb}$  and  $^{84}\text{Kr}$ . Note that  $[\epsilon^{(p)}(^1g_{9/2}), \epsilon^{(n)}(^1g_{9/2})] = [3.5, 1.5] \text{ MeV}$  for  $^{84}\text{Sr}$  and  $^{84}\text{Rb}$  nuclei and  $[\epsilon^{(p)}(^1g_{9/2}), \epsilon^{(n)}(^1g_{9/2})] = [1.5, 1.5] \text{ MeV}$  for  $^{84}\text{Kr}$ . In the figures circles represent protons and crosses represent neutrons. The Hartree-Fock energy ( $E$ ) in MeV, mass quadrupole moment ( $Q$ ) in units of the square of the oscillator length parameter and the total  $K$  quantum number of the lowest intrinsic states are given in the figure. See text for details.

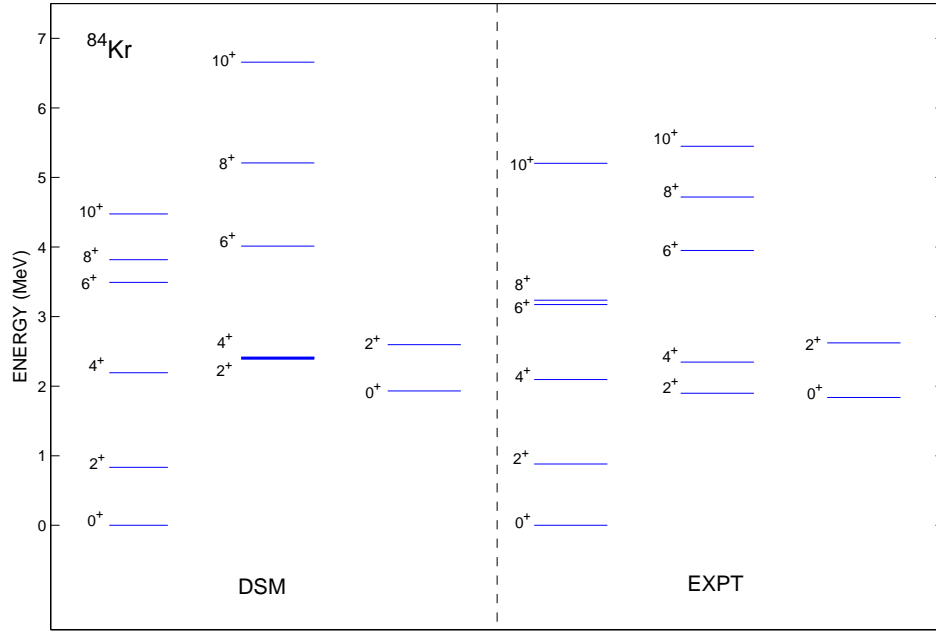


FIG. 4: (a) Calculated and (b) experimental spectra for  $^{84}\text{Kr}$ . The experimental data are from [43]. See text for details.